The Astrophysical Journal Letters, 878:L24 (5pp), 2019 June 10 https://doi.org/10.3847/2041-8213/ab25f4

Inner Heliosheath Shocks and Their Effect on Energetic Neutral Atom Observations by *IBEX*

P. Mostafavi[1,2], G. P. Zank[2], E. J. Zirnstein[1], and D. J. McComas[1]
[1] Department of Astrophysical Sciences, Princeton University, Princeton, NJ 08544, USA
[2] Department of Space Science, University of Alabama in Huntsville, Huntsville, AL 35805, USA
Received 2019 April 8; revised 2019 May 19; accepted 2019 May 21; published 2019 June 12

Abstract

A collision between an interplanetary disturbance in the solar wind and the heliospheric termination shock leads to the generation and propagation of plasma structures in the inner heliosheath (IHS). This interaction can lead to one or more shocks propagating in the IHS until they collide with the heliopause (HP). IHS shocks are (1) partially reflected at the HP and propagate back into the IHS and (2) partially transmitted into the very local interstellar medium. The IHS is dominated by the pressure of energetic particles as was observed by the Low Energy Charged Particle instrument on *Voyager 2* and by remote observations from *Interstellar Boundary Explorer* (*IBEX*), making the plasma beta, when the energetic particle pressure is included, much greater than one. We model IHS shocks using a pickup ion (PUI)-mediated plasma model and show that they are mediated by PUIs. The dissipation mechanism at perpendicular IHS shocks results primarily in PUIs being heated. Only a very small percentage of the upstream solar wind flow energy is converted to heating of lower energy solar wind ions at the shock. IHS shocks are broad because the diffusion coefficient associated with PUIs is large. The presence of IHS shocks results in greater heating of the PUI component in the IHS. The increased temperature enhances the production of energetic neutral atoms (ENAs) due to charge exchange between IHS PUIs and interstellar neutral gas. When IHS shocks are included in the model, we find that the predicted enhancement of the ENA flux leads to better consistency with corresponding *IBEX* observations.

Key words: ISM: atoms – shock waves – solar wind – Sun: heliosphere

1. Introduction

The Sun continuously emits solar wind ions that propagate supersonically into the heliosphere until they reach the heliospheric termination shock (HTS). The HTS and the inner heliosheath (IHS), a region of heated thermal solar wind ions and energetic particles between the HTS and the heliospheric boundary (heliopause (HP)), have been explored by *Voyager 1* and *2*. *Voyager 1* crossed the HTS at 94 au in 2004 (Stone et al. 2005), whereas the *Voyager 2* crossing was at 84 au in 2007 (Stone et al. 2008). Unfortunately, there are no observations during the *Voyager 1* crossing due to a data gap. *Voyager 2* crossed the HTS during a period when all instruments were working properly, including the plasma instrument, and were able to return data. The measurements taken by *Voyager 2* at the HTS crossing revealed that a small percentage of the upstream solar wind flow energy is converted to downstream heating of the thermal solar wind plasma (Richardson et al. 2008). The observed temperature of the thermal plasma downstream of the HTS was much less than the temperature anticipated by the magnetohydrodynamic (MHD) models (Pogorelov et al. 2009; Zank et al. 2009). It was predicted by Zank et al. (1996) that most of the upstream kinetic energy will be dissipated in heating the pickup ions (PUIs). PUIs, which are produced through charge exchange between interstellar neutral atoms and thermal solar wind ions in the heliosphere, are not equilibrated with the thermal ions. Reflected PUIs at the cross-shock electrostatic potential of the HTS provide significant amounts of dissipative heating of the bulk flow (Zank et al. 1996, 2010; Burrows et al. 2010; Lembege & Yang 2016; Mostafavi et al. 2017a, 2018, 73 Kumar et al. 2018). Zank et al. (2010) studied the microphysics of the HTS and computed the temperature of reflected and transmitted PUIs downstream of the HTS. Mostafavi et al. (2017a, 2017b) and Zank et al. (2018) used a PUI-mediated plasma model to investigate the structure of the HTS, finding preferential heating of PUIs compared to the thermal solar wind ions.

Decker et al. (2015), using the Low Energy Charged Particle instrument on *Voyager 2*, showed that the IHS, when accounting for anomalous cosmic rays/energetic particles with energies more than 28 keV, produces a plasma beta greater than one. Even though *Voyager* cannot measure PUIs, based on the low thermal solar wind pressure downstream of the HTS, we know that the IHS is dominated by PUIs (Zank et al. 1996). Zank et al. (2017) considered the PUI pressure in the IHS and estimated the plasma beta to be about 14 (with the inclusion of only thermal solar wind ions and PUIs). Thus, any shocks propagating in the IHS should be mediated by PUIs, and PUIs may be the primary dissipation mechanism for quasi-perpendicular IHS shocks.

Some fraction of the PUIs in the IHS undergo charge exchange with interstellar neutral atoms and become energetic neutral atoms (ENAs). These ENAs move freely across the magnetic field and some propagate into the heliosphere and can be detected by the *Interstellar Boundary Explorer* (*IBEX*) spacecraft located near the Earth at 1 au (McComas et al. 2009a). The *IBEX* mission images part of the ENAs distribution function that propagates from the outer heliosphere and the local interstellar medium (LISM). ENAs originating primarily from the IHS form the globally distributed flux (McComas et al. 2009b; Schwadron et al. 2014) and are the focus of this paper. Multiple studies have used the theory of ion acceleration at the HTS from Zank et al. (2010) to simulate PUIs in the IHS. Zank et al. (2010) only considered PUIs from the supersonic solar wind and assumed that the number density and temperature of particles in the IHS are constant. Desai et al. (2012) compared modeled ENA spectra from Zank et al. (2010)

to *IBEX* observations from ∼0.5 to 5 keV, finding that the transmitted PUI population contributes to most of the ENA flux between 0.5 and 5 keV, corresponding to the *IBEX*-Hi energy range. Desai et al. (2014) extended Desai et al. (2012) to include ENAs produced from PUIs outside the HP, which could contribute significantly to ENA fluxes below ∼0.5 keV. Zirnstein et al. (2014), accounting for the loss of energetic PUIs by charge exchange as they flow through the IHS, showed that PUIs from outside the HP could contribute a significant number of ENAs from ∼0.02 to 10 keV. However, there appears to be a discrepancy between recent modeling results and *IBEX* ENA observations, as recent models calculate fluxes a factor of ∼2–3 times lower (Zirnstein et al. 2017). A potential solution for this problem is the energization of PUIs by, e.g., turbulence in the IHS, which could account for this missing flux (Zirnstein et al. 2018a, 2018b). In this study, we aim to show that shocks propagating through the IHS can also account for at least part this missing flux.

Shock waves during solar minimum generally result from fast solar wind streams overtaking slower ones. The fast-slow solar wind stream interaction yields corotating interaction regions (CIRs) that are bounded by a forward and reverse shock (Pizzo 1978; Gosling & Pizzo 1999). Strong shock waves reach the IHS during solar minimum less frequently than during solar maximum. During solar maximum, the Sun is more active and produces many coronal mass ejections (CMEs) in which fast CMEs generally have strong leading shocks. Strong shocks produced during either solar minimum or maximum will eventually collide with the HTS, driving the HTS outward initially and generating propagating plasma structures in the IHS as shown by Story & Zank (1995, 1997), Zank et al. (2001), Zank & Muller (2003), Washimi et al. (2011), and Provornikova et al. (2012). These authors showed that the transmission of a shock wave across the HTS produces a weakened transmitted shock propagating in the IHS, along with an advected tangential or contact discontinuity. An IHS shock wave propagates through the IHS until it reaches the HP, when it is partially reflected back into the subsonic IHS, and partially transmitted into the very local interstellar medium (VLISM; Zank & Muller 2003; Washimi et al. 2011, 2012). Burlaga et al. (2013) identified an interplanetary transmitted shock in the VLISM using *Voyager 1* observations. Mostafavi & Zank (2018a, 2018b) showed that the 2012 shock in the VLISM was collisional with respect to the thermal gas and its structure was extremely broad.

Here, we use a PUI-mediated plasma model (Zank et al. 2014, 2016) to describe the structure of IHS shocks and show that the IHS shocks are mediated by suprathermal PUIs. PUIs introduce a collisionless heat conduction and viscosity (dissipation) in the IHS, and these processes are responsible for determining the structure of IHS shocks. Thus, similar to the HTS (Mostafavi et al. 2017a, 2017b; Zank et al. 2018), the primary dissipation mechanism at quasi-perpendicular IHS shocks is not provided by thermal solar wind ions, but PUIs. We estimate the diffusion length scale associated with PUIs in the IHS to be about 0.1–0.3 au. Because PUIs appear to be the dominant plasma component energetically in the IHS (Decker et al. 2015; Zank et al. 2017), PUIs are likely to be the primary component responsible for dissipation at a shock, and hence the diffusion length scale associated with PUIs will determine the thickness of shocks in the IHS. The propagation of interplanetary shocks into the IHS results in further heating of PUIs and, consequently, the more effective production of ENAs due to charge exchange between interstellar neutral gas and hot IHS PUIs. Thus, the inclusion of IHS shocks predicts an enhancement of the ENA flux, which improves the agreement with *IBEX* observations compared to previous models that neglect the dynamics of shocks in the IHS.

This Letter is organized as follows. We first briefly summarize the PUI-mediated plasma model used to study the structure of IHS shocks. In Section 3, we model IHS shocks and estimate the resulting enhanced ENA flux at 1 au and compare it to *IBEX* observations. Finally, we discuss and summarize our results.

2. Model

Zank et al. (2014, 2016) showed that PUIs in the IHS are not equilibrated with the background thermal solar wind ions and they therefore should be treated as a separate component in the system. We use the PUI-mediated plasma model presented by Zank et al. (2014) which is a two-fluid model that includes nonthermal PUIs, the thermal solar wind plasma, and the magnetic field. We aim to study the structure of collisionless shock waves in the IHS. PUIs experience pitch-angle scattering because of scattering off magnetic field fluctuations, which introduces a collisionless heat flux and a collisionless viscosity in the system. We therefore include both collisionless dissipation terms (heat flux and viscosity) associated with PUIs. The collisionless diffusion coefficient associated with PUIs in the IHS can be estimated by $K_p = \frac{1}{3}U_1{}^2\frac{B^2}{\langle \delta B^2\rangle}\tau_s$. The PUI pitch-angle scattering timescale, τ_s, in the IHS is calculated to be $\sim 2.6 \times 10^4$ s, which gives a diffusion coefficient of about $1.6 \times 10^{16}\,\mathrm{m^2\,s^{-1}}$. The approximate value of the PUI viscosity is $\sim P_p\tau_s = 3 \times 10^{-9}\,\mathrm{kg\,m^{-1}\,s^{-1}}$, which yields a PUI Schmidt number (i.e., the ratio between PUI collisionless viscosity and heat flux) of about 0.05. Based on these values, PUI dissipation terms are large (similar to the HTS; Mostafavi et al. 2017a), and PUIs will be heated preferentially, and the thermal solar wind will behave essentially adiabatically and remain relatively unheated.

Most IHS shocks in the nose direction are quasi-perpendicular because of the Parker spiral structure of the magnetic field in the distant heliosphere. The structure of a steady PUI-mediated collisionless perpendicular shock is governed by (Mostafavi et al. 2018)

$$\frac{d^2y}{d\bar{x}^2} + \frac{3}{\mathrm{Sch}_p}\left[\left(\frac{1}{M_{s1}^2}\left(\frac{1}{y}\right)^{\gamma_g+1} - 1\right) - \mathrm{Sch}_p y + \frac{y_B}{y^3}\right]\frac{dy}{d\bar{x}} = \frac{9\gamma_p}{\mathrm{Sch}_p\gamma_g M_{s1}^2}(1-y)V(y), \quad (1)$$

where

$$V(y) = \gamma_g M_{s1}^2\frac{\gamma_p+1}{2\gamma_p}\left(y - \frac{\gamma_p-1}{\gamma_p+1}\right) - \left(1 + \frac{P_{p1}}{P_{g1}} - \frac{(\gamma_g-\gamma_p)(1-y^{1-\gamma_g})}{\gamma_p(\gamma_g-1)(1-y)} - \gamma_g M_{s1}^2\frac{y_B}{2y}\left(\frac{\gamma_p-2}{\gamma_p} - y\right)\right). \quad (2)$$

Here, $M_{s1}^2 = \rho_1 U_1/\gamma_g P_{g1}$ is the thermal solar wind Mach number of the flow upstream of the shock, ρ is the total density,

U is the bulk flow velocity, and y the inverse compression ratio. All quantities pertaining to PUIs and thermal solar wind are denoted by the subscript p and g, respectively. $\gamma_{p/g}$ and $P_{p1/g1}$ are the adiabatic indices and far upstream pressure of the PUIs/thermal solar wind, respectively. $\bar{x}$ is the distance normalized to the PUI diffusion length scale K/U, and Sch_p is the Schmidt number. The square of the inverse Alfvén Mach number far upstream is y_B.

3. Results

We use the set of equations described in the last section to study the structure of perpendicular shock waves in the IHS. Zank et al. (2010) estimated that the suprathermal PUIs inside the IHS have a number density of about 25% of the thermal solar wind density. They therefore contribute a large pressure compared to the thermal plasma ($P_{p1}/P_{g1} \sim 24.9$; Mostafavi et al. 2018).

We need to estimate the shock propagation speed to simulate an IHS shock. Most shocks in the outer heliosphere are of the fast forward type (Rice & Zank 1999). Thus, we consider fast-mode shocks in the IHS that have a propagation speed that exceeds the magnetosonic speed of the region. We assume shocks in the IHS that have a compression ratio that is less or greater than 2 to be weak or strong shocks, respectively (Zank et al. 2001; Wang & Richardson 2003). Then, we model a strong and weak shock with in the IHS, using upstream parameters $\gamma_p = \gamma_g = 5/3$, $\frac{P_{p1}}{P_{g1}} = 24.9$, and solve Equation (1) in the stationary frame of the shock. We use a thermal solar wind density and average magnetic field strength in the IHS of about 0.0028 cm^{-3} and 0.12 nT, respectively (Burlaga et al. 2018). The dotted curves on Figures 1(a)–(c) show an example of a strong IHS shock with $M_{s1} = 10.3$ and $y_B = 0.013$. The PUI and thermal gas temperature as a function of distance are shown in Figure 1(a). The plot shows a smooth transition connecting the upstream to the downstream state with the compression ratio of 2.25. The magnetic field magnitude in Figure 1(b) shows that the thickness of the shock is broad and about 0.22 au, which is determined by PUI diffusion length scale. Figure 1(c) illustrates the thermal gas, magnetic, and PUI pressure as a function of distance. The shock is mediated by the PUI pressure, which is the dominant component upstream and downstream of the shock in the IHS. As at the HTS, the thermal gas does not contribute a large downstream pressure. An example of a weak IHS shock with $M_{s1} = 7.87$ and $y_B = 0.023$ is shown in the solid curves of Figures 1(a)–(c). The PUI, thermal gas temperature, and magnetic field magnitude as a function of distance show a smooth transition with a compression ratio of 1.75 (Figures 1(a) and (b)). The thickness of this shock, as determined by PUI diffusion length scale, is about 0.14 au. Figure 1(c) shows that the weak IHS shock is mediated by suprathermal PUIs. The figures show that the scale length is determined by the large diffusion coefficient associated with PUIs. Therefore, shocks in the IHS are broad with a thickness that is ~0.1–0.3 au depending on their strength. No published detailed analysis exists regarding observations of the IHS shocks. On applying the magnetometer data to shocks in the IHS, we can calculate the shock thickness by multiplying the thickness of these shocks in days by the average shock speed in the IHS, which yields a shock thickness of ~0.1–0.3 au.

Next, we estimate the ENA flux that *IBEX* might observe at 1 au when shocks are present in the IHS. We have used the first

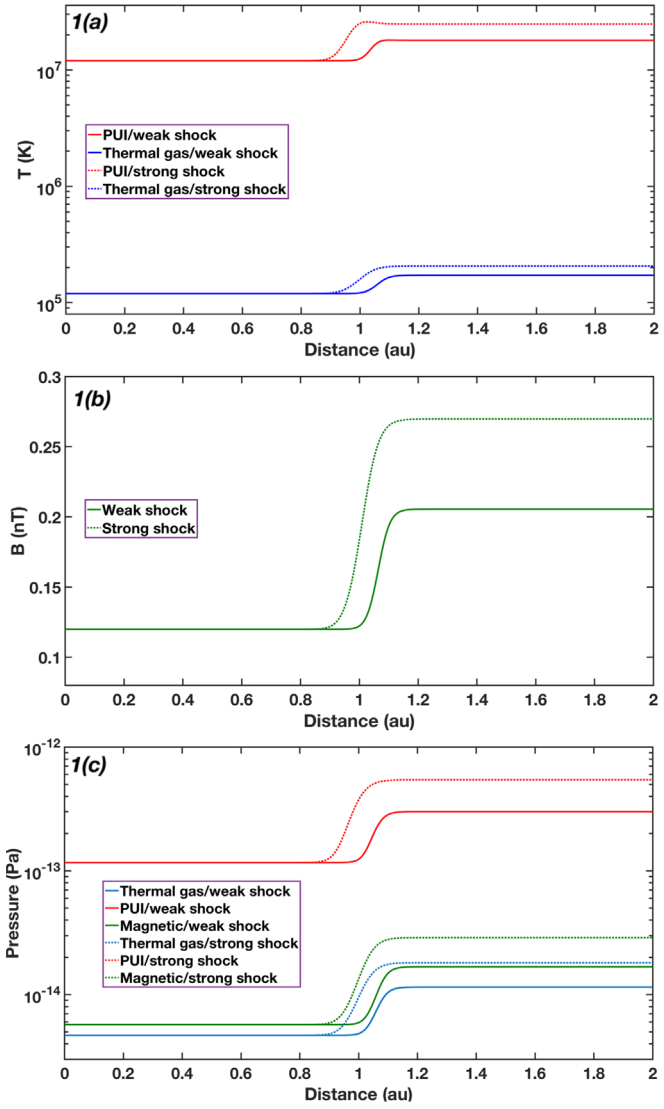

Figure 1. Smoothed shock transition corresponding to perpendicular shocks in the IHS when both the PUI heat flux and viscosity are included. Here, $\gamma_p = \gamma_g = 5/3$ and $P_{p1}/P_{g1} = 24.9$. A strong IHS shock with $M_{s1} = 10.3$, and $y_B = 0.013$ and a weak IHS shock with $M_{s1} = 7.87$, and $y_B = 0.023$ are plotted with a dotted curve and a solid curve, respectively. (1a) PUI and thermal gas temperature and (1b) magnetic field magnitude (nT), through the strong IHS shock as a function of distance. (1c) PUI, thermal gas, and magnetic pressure as a function of distance.

5 yr average of the ENA flux observed by *IBEX* (McComas et al. 2014), statistically combining nine $6^\circ \times 6^\circ$ pixels nearest to the *Voyager 1* direction. During the first few years, *IBEX* maps generally reflect solar minimum conditions. During solar minimum the number of shocks propagating in the heliosphere is less than solar maximum. We assume that there are at least two shocks propagating in the IHS all the time (based on the Washimi et al. 2012 model). The approximate transit time of a shock across the IHS is about 5–6 months, depending on its speed.

In order to model the ENA flux along the *Voyager 1* direction in the IHS, we construct the total proton distribution downstream of the HTS by taking the upstream shock values for the thermal ion and PUI populations from Figure 1. We calculate a total density of 0.0035 cm^{-3} and effective temperature 2.5×10^6 K. We assume that the combined thermal solar wind ion and PUI distribution just downstream

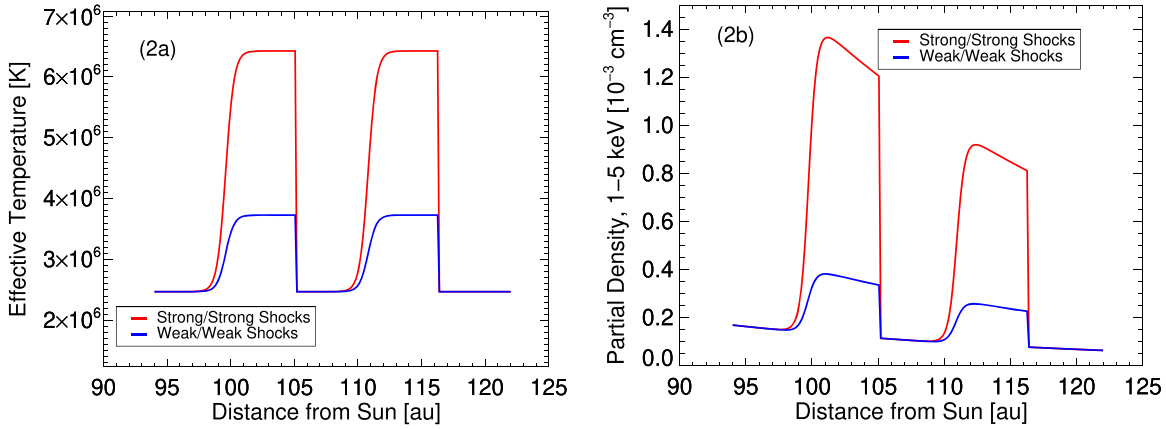

Figure 2. Example of the proton IHS effective temperature (2a) and proton partial density at 1–5 keV (2b) when two shocks are present in the IHS.

of the HTS is a kappa distribution with kappa index = 2 (Livadiotis et al. 2011). Then, we propagate the proton distribution through the IHS while taking into account losses by charge exchange with interstellar neutral atoms, according to (Fahr et al. 2007)

$$f(r, v) = f(r_{\rm HTS}, v)\exp\left(-\int_{r_{\rm HTS}}^{r} n_H \sigma(v_{\rm rel}) v_{\rm rel} \frac{dr}{u}\right), \quad (3)$$

where $r_{\rm HTS}$ is the distance to the HTS, $n_{\rm H} = 0.1\,{\rm cm}^{-3}$ is the interstellar neutral hydrogen density (e.g., Bzowski et al. 2009), $u = 40\,{\rm km\,s}^{-1}$ is the average solar wind bulk flow speed observed by *Voyager 1* in the IHS (e.g., Krimigis et al. 2011), $v_{\rm rel}$ is the relative speed of interaction between protons and interstellar neutral atoms given by (e.g., Chalov et al. 2003)

$$v_{\rm rel}(v < u) = u + \frac{v^2}{3u}$$
$$v_{\rm rel}(v > u) = v + \frac{u^2}{3v} \quad (4)$$

and σ is the energy-dependent, charge-exchange cross section (Lindsay & Stebbings 2005). The proton effective temperature is enhanced at the locations of the shocks shown in Figure 2(a), with their corresponding partial density at 1–5 keV shown in Figure 2(b). We consider the possibilities of two weak shocks or two strong shocks in the IHS (blue curves and red curves in Figure 2, respectively).

The ENA model results and observations by *IBEX* in the *Voyager 1* direction at 1 au for both cases of IHS with two shocks are plotted in Figure 3. The presence of shock waves in the IHS increases the IHS PUI temperature primarily, which leads to an increased production of ∼keV ENAs from the IHS. The number of ENAs in the presence of shock waves is increased and the predicted ENA flux is in a better agreement with the observed *IBEX* ENA flux. Thus, the difference between *IBEX* observations and previous models may be explained in part by considering the energization of PUIs by shock waves in the IHS. In Figure 3, we show some different possible cases of shocks in the IHS. The blue curve shows the case when two weak shocks are present in the IHS, and the red curve shows the IHS with two strong shocks. Strong shocks are not always present in the IHS, especially during solar minimum. The presence of a strong and weak shock in the IHS gives the ENA flux with the green curve. This curve is

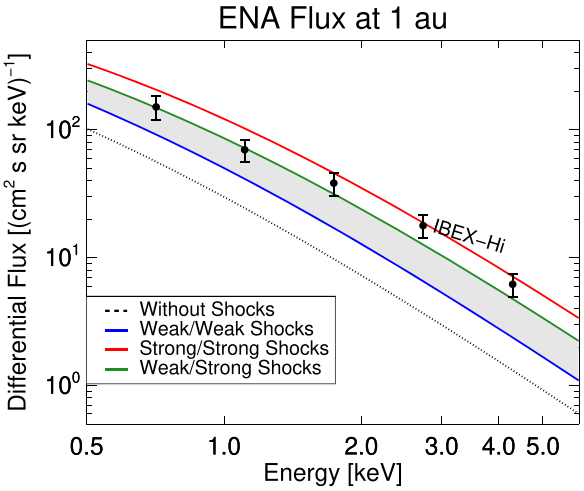

Figure 3. Energy spectrum of ENAs at 1 au in the *Voyager 1* direction. All fluxes have been survival-probability corrected for ENA losses within 100 au of the Sun. Black dots represent the ENA flux from the five energy channels of *IBEX*-Hi. The black dashed curve shows the ENA flux in the absence of shocks in the IHS. The blue and red curves show the ENA flux in the presence of two weak shocks and two strong shocks in the IHS, respectively. The green curve shows a case with one weak and one strong shock in the IHS. The gray region (between the green and blue curves) shows an estimate of the ENA flux during solar minimum.

very consistent with *IBEX*-Hi observations. The gray region represents an estimation of the ENA flux during the solar minimum (the estimation is based on Washimi et al. 2012). Thus, this result shows that shocks in the IHS provide an extra source of PUI energization and only by increasing the net PUI temperature in the IHS, may be responsible for some part of the missing ENA flux. Other mechanisms, such as turbulence, might also be another source of PUI energization in the IHS, as shown by Zirnstein et al. (2018a, 2018b).

4. Conclusions

Shocks propagate continuously through the IHS because of the interaction between the HTS and interplanetary disturbances with an increased pressure or density. The IHS is a subsonic region that leads to the partial reflection of shocks after their collision with the HP. Thus, the presence of shocks in the IHS should not be ignored in modeling and analyzing outer heliospheric observations. The IHS is thermally dominated by energetic PUIs that mediate shocks propagating in this

region. We have shown that shocks in the IHS are broad because of the large diffusion coefficient associated with PUIs. This results in further heating of the PUI component in the IHS, rather than heating of the subsonic thermal solar wind plasma. The IHS temperature is therefore increased further by transmitted interplanetary shocks, which results in the more effective production of ∼keV ENAs. We have shown that the production of ENAs in the presence of shocks in the IHS yields better consistency with the observed *IBEX* ENA flux at 1 au.

P.M. acknowledges the support of a NASA Earth and Space Science Fellowship Program Grant 16-HELIO16F-0022. G.P.Z. acknowledges partial support by the NSF/DOE Partnership in Basic Plasma Science and Engineering via NSF grant PHY-1707247 and a NASA award NNX14AJ53G. G.P.Z. has also been supported in part by the NSF EPSCoR RII-Track-1 Cooperative Agreement OIA-1655280, and *IBEX* subaward SUB 0000167/NASA 80NSSC18k0237. E.J.Z. acknowledges partial support from NASA grant NNX16AG83G. This work was also carried out as part of the *IBEX* mission, which is a part of the NASA Explorer Program (NNG17FC93C; NNX17AB04G). We thank Dr. Tae Kim for useful discussions.

ORCID iDs

P. Mostafavi https://orcid.org/0000-0002-3808-3580
G. P. Zank https://orcid.org/0000-0002-4642-6192
E. J. Zirnstein https://orcid.org/0000-0001-7240-0618
D. J. McComas https://orcid.org/0000-0002-9745-3502

References

Burlaga, L. F., Ness, N. F., Gurnett, D. A., & Kurth, W. S. 2013, ApJL, 778, L3
Burlaga, L. F., Ness, N. F., & Richardson, J. D. 2018, ApJ, 861, 9
Burrows, R. H., Zank, G. P., Webb, G. M., Burlaga, L. F., & Ness, N. F. 2010, ApJ, 715, 1109
Bzowski, M., Möbius, E., Tarnopolski, S., Izmodenov, V., & Gloeckler, G. 2009, SSRv, 143, 177
Chalov, S. V., Fahr, H. J., & Izmodenov, V. V. 2003, JGR, 108, 1266
Decker, R. B., Krimigis, S. M., Roelof, E. C., & Hill, M. E. 2015, JPhCS, 577, 012006
Desai, M. I., Allegrini, F. A., Bzowski, M., et al. 2014, ApJ, 780, 98
Desai, M. I., Allegrini, F. A., Dayeh, M. A., et al. 2012, ApJL, 749, L30
Fahr, H.-J., Fichtner, H., & Scherer, K. 2007, RvGeo, 45, RG4003
Gosling, J. T., & Pizzo, V. J. 1999, SSRv, 89, 21
Krimigis, S. M., Roelof, E. C., Decker, R. B., & Hill, M. E. 2011, Natur, 474, 359
Kumar, R., Zirnstein, E. J., & Spitkovsky, A. 2018, ApJ, 860, 156
Lembege, B., & Yang, Z. 2016, ApJ, 827, 73
Lindsay, B. G., & Stebbings, R. F. 2005, JGR, 110, A12213
Livadiotis, G., McComas, D. J., Dayeh, M. A., Funsten, H. O., & Schwadron, N. A. 2011, ApJ, 734, 1
McComas, D. J., Allegrini, F., Bochsler, P., et al. 2009a, Sci, 326, 959
McComas, D. J., Allegrini, F., Bochsler, P., et al. 2009b, SSRv, 146, 11
McComas, D. J., Allegrini, F., Bzowski, M., et al. 2014, ApJS, 213, 20
Mostafavi, P., & Zank, G. P. 2018a, JPhCS, 1100, 012018
Mostafavi, P., & Zank, G. P. 2018b, ApJL, 854, L15
Mostafavi, P., Zank, G. P., & Webb, G. M. 2017a, JPhCS, 900, 012016
Mostafavi, P., Zank, G. P., & Webb, G. M. 2017b, ApJ, 841, 4
Mostafavi, P., Zank, G. P., & Webb, G. M. 2018, ApJ, 868, 120
Pizzo, V. 1978, JGR, 83, 5563
Pogorelov, N. V., Borovikov, S. N., Zank, G. P., & Ogino, T. 2009, ApJ, 696, 1478
Provornikova, E., Opher, M., Izmodenov, V., & Toth, G. 2012, ApJL, 756, L37
Rice, W. K. M., & Zank, G. P. 1999, JGR, 104, 12563
Richardson, J. D., Kasper, J. C., Wang, C., Belcher, J. W., & Lazarus, A. J. 2008, Natur, 454, 63
Schwadron, N. A., Moebius, E., Fuselier, S. A., et al. 2014, ApJS, 215, 13
Stone, E. C., Cummings, A. C., McDonald, F. B., et al. 2005, Sci, 309, 2017
Stone, E. C., Cummings, A. C., McDonald, F. B., et al. 2008, Natur, 454, 71
Story, T. R., & Zank, G. P. 1995, JGR, 100, 9489
Story, T. R., & Zank, G. P. 1997, JGR, 102, 17381
Wang, C., & Richardson, J. D. 2003, AIP Conf. Ser. 679, Solar Wind Ten, ed. M. Velli et al. (Melville, NY: AIP), 725
Washimi, H., Webber, W., Zank, G. P., et al. 2012, ApJL, 757, L2
Washimi, H., Zank, G. P., Hu, Q., et al. 2011, MNRAS, 416, 1475
Zank, G. P., Adhikari, L., Zhao, L.-L., et al. 2018, ApJ, 869, 23
Zank, G. P., Du, S., & Hunana, P. 2017, ApJ, 842, 114
Zank, G. P., Heerikhuisen, J., Pogorelov, N. V., Burrows, R., & McComas, D. 2010, ApJ, 708, 1092
Zank, G. P., Hunana, P., Mostafavi, P., & Goldstein, M. L. 2014, ApJ, 797, 87
Zank, G. P., Mostafavi, P., & Hunana, P. 2016, JPhCS, 719, 012014
Zank, G. P., & Muller, H.-R. 2003, in AIP Conf. Ser. 679, Solar Wind Ten, ed. M. Velli et al. (Melville, NY: AIP), 762
Zank, G. P., Pauls, H. L., Cairns, I. H., & Webb, G. M. 1996, JGR, 101, 457
Zank, G. P., Pogorelov, N. V., Heerikhuisen, J., et al. 2009, SSRv, 146, 295
Zank, G. P., Rice, W. K. M., Cairns, I. H., et al. 2001, JGR, 106, 29363
Zirnstein, E. J., Heerikhuisen, J., Zank, G. P., et al. 2014, ApJ, 783, 129
Zirnstein, E. J., Heerikhuisen, J., Zank, G. P., et al. 2017, ApJ, 836, 238
Zirnstein, E. J., Kumar, R., Heerikhuisen, J., McComas, D. J., & Galli, A. 2018a, ApJ, 865, 150
Zirnstein, E. J., Kumar, R., Heerikhuisen, J., McComas, D. J., & Galli, A. 2018b, ApJ, 860, 170